Rock and Soil Mechanics

Volume 44 | Issue 3 Article 2

7-21-2023

Long-term deformation test and model study of one-dimensional consolidation of South China Sea coral mud under graded loading and unloading

Yang SHEN
Key Laboratory of Geomechanics and Embankment Engineering of Ministry of Education, Hohai University, Nanjing, Jiangsu 210098, China

Jue DENG
Key Laboratory of Geomechanics and Embankment Engineering of Ministry of Education, Hohai University, Nanjing, Jiangsu 210098, China

He WENG
Key Laboratory of Geomechanics and Embankment Engineering of Ministry of Education, Hohai University, Nanjing, Jiangsu 210098, China

Long YANG
Key Laboratory of Geomechanics and Embankment Engineering of Ministry of Education, Hohai University, Nanjing, Jiangsu 210098, China

Recommended Citation

SHEN, Yang; DENG, Jue; WENG, He; and YANG, Long (2023) "Long-term deformation test and model study of one-dimensional consolidation of South China Sea coral mud under graded loading and unloading," *Rock and Soil Mechanics*: Vol. 44: Iss. 3, Article 2.
DOI: 10.16285/j.rsm.2022.5528
Available at: https://rocksoilmech.researchcommons.org/journal/vol44/iss3/2

Rock and Soil Mechanics 2023 44(3): 685−696 ISSN 1000−7598
https: //doi.org/10.16285/j.rsm.2022.5528 http://rocksoilmech.researchcommons.org/journal

Long-term deformation test and model study of one-dimensional consolidation of South China Sea coral mud under graded loading and unloading

SHEN Yang, DENG Jue, WENG He, YANG Long
Key Laboratory of Geomechanics and Embankment Engineering of Ministry of Education, Hohai University, Nanjing, Jiangsu 210098, China

Abstract: South China Sea coral mud is a calcareous ooze of marine rock and soil formed by the accumulation of bones and debris after the death of coral groups, which has special engineering properties. It is significant to investigate its time dependent long-term nonlinear deformation under load for the construction and long-term stability analysis of dredger fill islands and reefs. Three groups of one-dimensional consolidation compression tests of coral mud with different loading and unloading schemes were carried out, and the influence of stress history on its long-term deformation properties was explored by changing the loading time and loading-unloading loops. According to the three-stage law of coral mud's instantaneous deformation, delayed attenuation deformation and delayed stable deformation under loading and unloading test conditions, the improved Burgers model was used to fit ε-t curves under different vertical stresses, which has high fitting accuracy. Meanwhile, after analyzing the model parameters, it was found that the instantaneous strain increment and its growth rate decrease with the increase of graded loading time, the duration of delayed attenuation under the final load decreases, and the delayed stable strain rate and the total strain increment under the final load decrease. In the same loading-unloading loops, the instantaneous strain increment in the unloading stage is smaller than that in the loading stage under the same vertical stresses. With the increase of loading-unloading loops, the instantaneous strain increment in each stage of loading and unloading decreases and is close to each other, the duration of delayed attenuation deformation, the delayed stable strain rate and total strain increment under the final load decrease. The effects of graded loading time and loading and unloading cycles on the long-term deformation properties of coral mud were studied to provide theoretical basis for surcharge preloading scheme in island reef construction.

Keywords: South China Sea coral mud; graded loading and unloading; long-term nonlinear deformation; improved Burgers model; model parameters

1 Introduction

China has promoted the construction of the 21st Century Maritime Silk Road in recent years under the Belt and Road initiative. And large scale reclamation projects on coral islands and reefs in the South China Sea are conducted at present[1]. As the main hydraulic fill material of the foundation, the South China Sea coral mud is the marine rock and soil formed by the debris accumulation after the death of coral colony in the long geological process. Its deformation under the overburden pressure is similar to the double drainage consolidation under 1D condition in relevant foundation researches. The South China Sea coral mud is characterized by its fragility, high void ratio, high internal friction angle, high compressibility, and special engineering properties, which is different from conventional terrigenous soil[2−3]. It is of great significance to investigate its long-term nonlinear deformation under load for the construction and long-term stability analysis of dredger fill islands and reefs.

Most soils, especially weak soil, exhibit time-dependent nonlinear deformation characteristics under constant vertical stress[4]. Two hypotheses are often used to investigate this long-term nonlinear deformation: hypothesis A and hypothesis B. Both of them purport that the long-term nonlinear deformation can be divided into the deformation caused by the pore water dissipation and the time-dependent deformation. Their differences are that hypothesis A purports that the time-dependent deformation only occurs after the pore water dissipation (such as Mesri et al.[5−7], Ladd et al.[8]). However, hypothesis B purports that the time-dependent deformation exists in the whole deformation process (such as Bjerrum[9], Graham et al.[10], Yin et al.[4, 11−14]). Based on hypothesis B, scholars have proposed many theories. Bjerrum[9] proposed a timeline model to estimate delayed consolidation by introducing instantaneous compression line and time line. Graham et al.[10] derived an elastic visco-plastic model to describe time-dependent stress−strain behavior using equivalent time concept based on Bjerrum[9]. Yin et al.[4] further developed the concept of equivalent time, and proposed an 1D elastic visco-plastic model. Feng et al.[15] conducted a loading and unloading oedometer test on marine sedimentary soil in Hong Kong

Received: 15 April 2022 Accepted: 23 July 2022
This work was supported by the National Natural Science Foundation of China (51979087).
First author: SHEN Yang, male, born in 1980, PhD, Professor, PhD supervisor, research interests: static and dynamic characteristics of soil and its constitutive theory. E-mail: shenyang1998@163.com

based on Yin et al.[4], and proposed a nonlinear elastic visco-plastic equation by considering the loading compression and unloading rebound. Hu et al.[16] used a hyperbolic function to fit the strain−stress isochronous curve of the sandy silted soil in Dongting Lake. Wang et al.[17] established an elastic visco-plastic model of coastal weak soil based on 1D stress−strain isochronous curve. Some scholars also used component model for analysis in the model development process. The component model combines the basic components in parallel and in series, and the actual soil deformation can be simulated by combining different component based on laboratory tests. Taylor et al.[18] used Kelvin model to describe visco-elastic deformation. Yin et al.[19] deduced a soft-matter element and its constitutive equations based on fractional calculus operator theory. Liu et al.[20] introduced the spring-pot component to modify the Kelvin model, and described the 1D constitutive relationship of saturated clay. Liu et al.[21] used Burgers model to simulate the instantaneous and delayed deformation process. Chen et al.[22] replaced the linear spring of the Merchant model with a nonlinear spring, and established a three-components nonlinear elastic-viscous model by combining Kelvin body in series.

Previous model researches have achieved good results in describing the long-term deformation characteristics of soil in the loading stage, while they were not widely used in the unloading stage, which is an important aspect that cannot be ignored when considering the preloading and unloading scheme in actual project. Therefore, the long-term deformation properties of coral mud in the loading-unloading stages are investigated through 1D oedometer tests with different loading and unloading schemes. According to the strain−time curve, the improved Burgers model was used to fit and determine the model parameters, the influence of graded loading time and the loading-unloading loops on the 1D long-term deformation of coral mud were analyzed based on its physical meaning. It will provide a basis for the preloading scheme.

2 Materials and instruments

2.1 Materials

The used South China Sea coral mud in the 1D oedometer test is sampled from the South China Sea. During the reclamation construction, calcareous silt interlayer will be formed due to the hydraulic sorting. The calcium carbonate content of the South China Sea coral mud is as high as 90%[23], and its color is white to light yellow. Its basic physical and mechanical properties are shown in Table 1.

Table 1 Basic physical and mechanical properties of South China Sea coral mud

Specific density G_s	Liquid limit ω_L /%	Plastic limit ω_p /%	Water content ω /%
2.77	33.8	23.0	45.5

Figure 1 shows the electronic scanning image of South China Sea coral mud obtained by SEM test, and its particle size distribution curve is showed in Fig. 2. The South China Sea coral mud has some features such as sharp edges, uneven distribution, strip and needle shapes, which is quite different from the general silt or weak clay. Since many internal pores exist, the coral mud are rapidly compressed at the loading moment, resulting in large instantaneous deformation. With the increase of loading time, the relative position of coral mud particles change slower than the general weak clay due to the irregular shape of particles, then longer time is needed to reach the stable deformation[2].

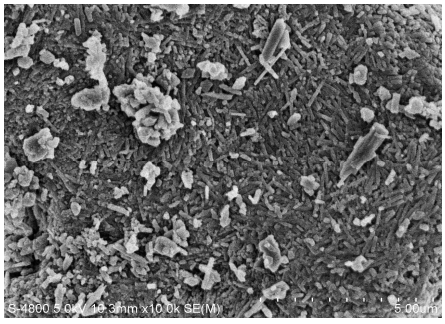

Fig. 1 Scanning electron microscope image of South China Sea coral mud

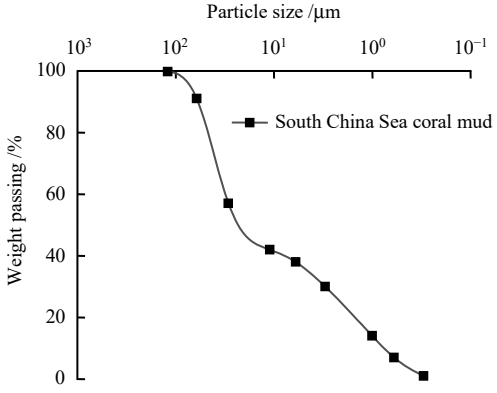

Fig. 2 Particle size distribution curve of South China Sea coral mud

2.2 Instrument

WG single-lever consolidation instrument, produced by Nanjing Soil Instrument Factory Co., Ltd., was employed

to conduct the 1D oedometer test. The sample is 20.0 mm high and 61.8 mm in diameter, and water can be drained at both sides. During the test, the water level in the tank was kept higher than that in the sample to ensure sample saturation. The initial void ratios of the samples are 1.26, 1.29, and 1.23 in the three test groups, with the initial water content of 45.36%, 46.61%, and 44.54%, respectively.

3 Test scheme

Three groups of 1D oedometer tests (T1, T2, and T3) were designed, and different loading time and loading-unloading methods were adopted, which corresponded to the different loading time and loading-unloading loops of the preloading method in the actual project, as shown in Table 2. Logarithmic time method was adopted for all three groups. The readings were recorded when lg$t$ = −1.0, −0.8, −0.6, −0.4..... (t is the loading time (min)). T1 test, the first 8 load levels in T2 test, and T3 test were used to investigate the effect of graded loading time on the 1D long-term deformation of coral mud, and T2 test was used to examine the effect of loading-unloading loops on the 1D long-term deformation of coral mud.

Table 2 Schemes of tests

No.	Test procedure	Vertical stress /kPa	Loading time /min	Test procedure	Vertical stress /kPa	Loading time /min	Test procedure	Vertical stress /kPa	Loading time /min
T1	1	25	10 080	4	200	10 080	7	1 600	10 080
	2	50	10 080	5	400	10 080	8	3 200	11 520
	3	100	10 080	6	800	10 080			
T2	1	25	1 440	14	200	1 440	27	1 600	1 440
	2	50	1 440	15	400	1 440	28	3 200	11 520
	3	100	1 440	16	800	1 440	29	1 600	1 440
	4	200	1 440	17	1 600	1 440	30	800	1 440
	5	400	1 440	18	3 200	11 520	31	400	1 440
	6	800	1 440	19	1 600	1 440	32	200	1 440
	7	1 600	1 440	20	800	1 440	33	100	1 440
	8	3 200	11 520	21	400	1 440	34	200	1 440
	9	1 600	1 440	22	200	1 440	35	400	1 440
	10	800	1 440	23	100	1 440	36	800	1 440
	11	400	1 440	24	200	1 440	37	1 600	1 440
	12	200	1 440	25	400	1 440	38	3 200	11 520
	13	100	1 440	26	800	1 440			
T3	1	25	10	4	200	10	7	1 600	10
	2	50	10	5	400	10	8	3 200	11 520
	3	100	10	6	800	10			

Note: 10, 1 440, 10 080, 11 520 min in Table are the loading time of each load level.

4 Results and analysis

4.1 1D long-term deformation characteristics in each loading-unloading stage

Figure 3 shows the strain−time (ε–t) curves of coral mud in T1, T2, and T3 tests in each loading-unloading stage, and its deformation is mainly divided into three stages. The ε–t curve is a steep straight line at each vertical stress moment, the instantaneous deformation is produced, and the strain rate is large. Subsequently, the ε–t curve becomes an arc with increasing time (convex upwards in loading stage and convex downwards in unloading stage), the strain rate of soil gradually decreases, and delayed attenuation deformation appears. Finally, the ε–t curve tends to be linear in the final deformation stage, and the strain rate of the soil gradually stabilizes and tends to be constant, the delayed stable deformation occurs at this moment.

4.2 Burgers model in loading and unloading stage

Coral mud demonstrates three-stage characteristics under all the vertical stress levels, ie. instantaneous deformation, delayed attenuation deformation, and delayed stable deformation, which is consistent with the basic features of the classical Burgers model curve[21]. Burgers model was adopted to fit the 1D consolidation strain−time curve in each loading and unloading stage. Burgers model combines Kelvin body (Hook spring is in parallel with Newton dashpot) and Maxwell body (Hook spring is in series with Newton dashpot) acting in series, as shown in Fig. 4.

When analyzing the Burgers model in the loading stage, the constitutive equation of Burgers model under the vertical stress is expressed as

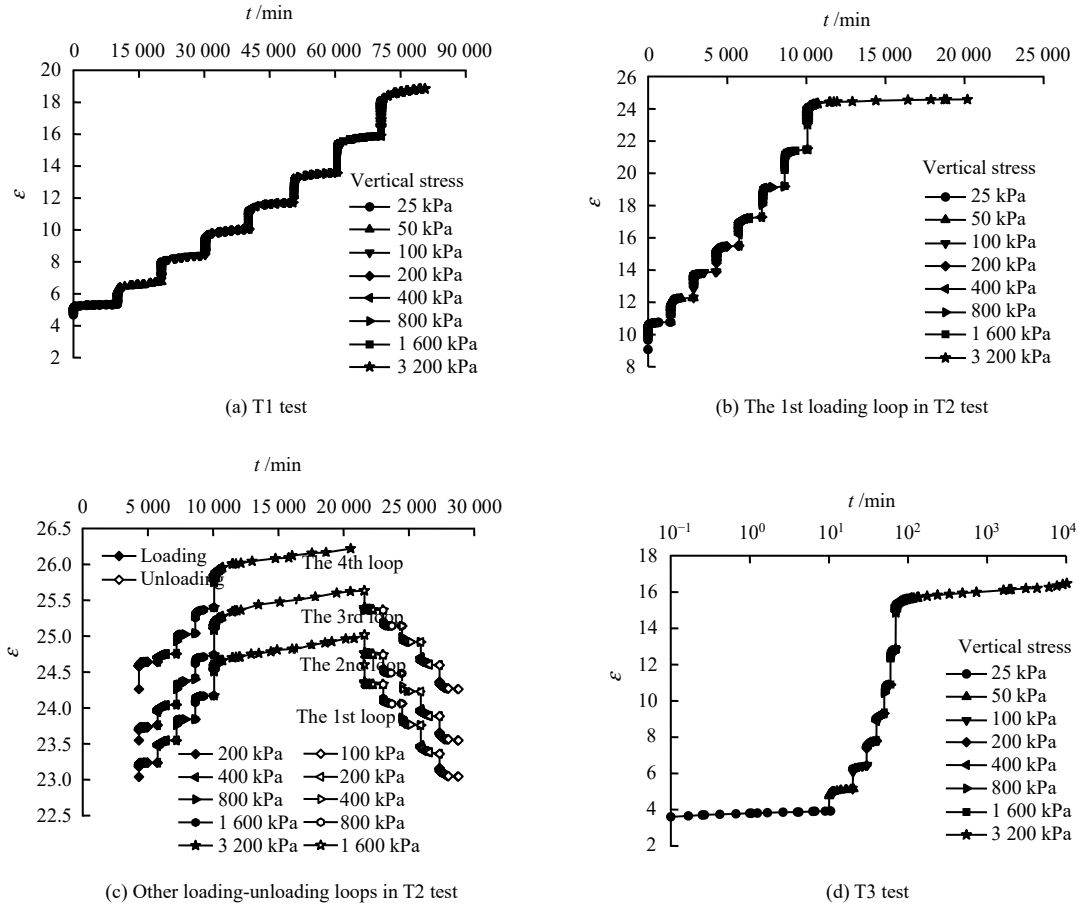

(a) T1 test

(b) The 1st loading loop in T2 test

(c) Other loading-unloading loops in T2 test

(d) T3 test

Fig. 3 ε–t curves in T1, T2 and T3 tests

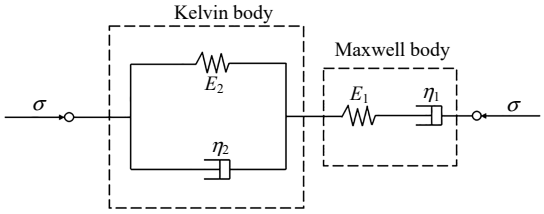

Fig. 4 Schematic diagram of Burgers model

$$\sigma+\left(\frac{\eta_1}{E_1}+\frac{\eta_1+\eta_2}{E_2}\right)\dot{\sigma}+\frac{\eta_1\eta_2}{E_1E_2}\ddot{\sigma}=\eta_1\dot{\varepsilon}+\frac{\eta_1\eta_2}{E_2}\ddot{\varepsilon} \tag{1}$$

where σ is the vertical stress of 1D oedometer test; E_1 and E_2 are the elastic modulus of spring; η_1 and η_2 are the viscosity coefficients of dashpots.

When the vertical stress σ is constant, Eq. (1) can be rewritten as

$$\varepsilon_{\mathrm{p}}(t)=\frac{\sigma}{E_1}+\frac{\sigma}{\eta_1}t+\frac{\sigma}{E_2}\left(1-\mathrm{e}^{-\frac{E_2}{\eta_2}t}\right) \tag{2}$$

where $\varepsilon_{\mathrm{p}}(t)$ is the strain of Burgers model in the loading stage.

Let $A=\dfrac{\sigma}{E_1}$, $B=\dfrac{\sigma}{\eta_1}$, $C=\dfrac{\sigma}{E_2}$, $D=\dfrac{E_2}{\eta_2}$, $\varepsilon_{\mathrm{p}}(t)$ of Eq. (2) can be written as

$$\varepsilon_{\mathrm{p}}(t)=A+Bt+C(1-\mathrm{e}^{-Dt}) \tag{3}$$

From the characteristics of Burgers model in the unloading stage, its constitutive equation is deduced in this paper, and Maxwell and Kelvin bodies are analyzed respectively. For Maxwell body, Eq. (4) can be obtained according to the initial conditions $\varepsilon(t)\big|_{t=0}=\sigma/E_1$ under constant vertical stress σ:

$$\varepsilon=\frac{\sigma}{E_1}+\frac{\sigma}{\eta_1}t \tag{4}$$

The graded unloading method was adopted, and the vertical stress $\Delta\sigma$ was removed to σ_1 at t_1 time, since the unloading ratio is 1, then $\Delta\sigma=\sigma_1=\sigma/2$. $\Delta\sigma$ is the removed vertical stress, σ_1 is the vertical stress after unloading, and t_1 is the unloading time. When $t\geqslant t_1$, the strain $\varepsilon_{\mathrm{Mr}}$ of Maxwell body in the unloading stage is

$$\varepsilon_{\mathrm{Mr}}=\frac{\sigma_1}{E_1}+\frac{\sigma}{\eta_1}t_1+\frac{\sigma_1}{\eta_1}(t-t_1) \tag{5}$$

For Kelvin body, the vertical stress $\Delta\sigma$ was removed to σ_1 at t_1 time, when $t\geqslant t_1$, the strain $\varepsilon_{\mathrm{Kr}}$ of Kelvin body in the unloading stage is

$$\varepsilon_{\mathrm{Kr}}=\frac{\sigma}{E_2}\left(1-\mathrm{e}^{-\frac{E_2}{\eta_2}t}\right)-\frac{\sigma-\sigma_1}{E_2}\left[1-\mathrm{e}^{-\frac{E_2}{\eta_2}(t-t_1)}\right] \tag{6}$$

So the strain of Burgers model in the unloading stage is

$$\varepsilon_{\mathrm{r}}=\varepsilon_{\mathrm{Mr}}+\varepsilon_{\mathrm{Kr}}=$$

$$\frac{1}{2}\left[\frac{\sigma}{E_1}+\frac{\sigma}{\eta_1}t_1+\frac{\sigma}{\eta_1}t+\frac{\sigma}{E_2}+\frac{\sigma}{E_2}\mathrm{e}^{-\frac{E_2}{\eta_2}(t-t_1)}-\frac{2\sigma}{E_2}\mathrm{e}^{-\frac{E_2}{\eta_2}t}\right] \quad (7)$$

Let $A=\frac{\sigma}{E_1}$, $B=\frac{\sigma}{\eta_1}$, $C=\frac{\sigma}{E_2}$, $D=\frac{E_2}{\eta_2}$, Eq. (7) can be rewritten as

$$\varepsilon_{\mathrm{r}}=\frac{1}{2}\left[A+Bt_1+Bt+C+C\mathrm{e}^{-D(t-t_1)}-2C\mathrm{e}^{-Dt}\right] \quad (8)$$

4.3 Determination of Burgers model parameters in loading-unloading stage

Equation (3) was used to fit the ε−t curves of T1, T2, and T3 tests in loading stage in Fig. 3, as shown in Fig. 5. Burgers model has a high fitting accuracy and can well reflect the characteristics of the instantaneous deformation, delayed attenuation deformation, and delayed stable deformation of coral mud in the loading stage.

The values of A, B, C, and D were obtained according to Fig. 5, then the Burgers model parameters E_1, E_2, η_1, η_2 of the T1, T2, and T3 tests under each vertical stress level in the loading stage could be determined, as shown in Fig. 6. Eqs. (3) and (8) are used to fit the ε–t curves under each vertical stress level in the loading-unloading stages of T2 test, and they were compared with the results of T2 test as the load increased from σ_i to σ_{i+1} (σ_i and σ_{i+1} are the load levels of the loading-unloading stages in T2 test) and that as the load decreased from σ_{i+1} to σ_i. The fitting results are shown in Fig. 7.

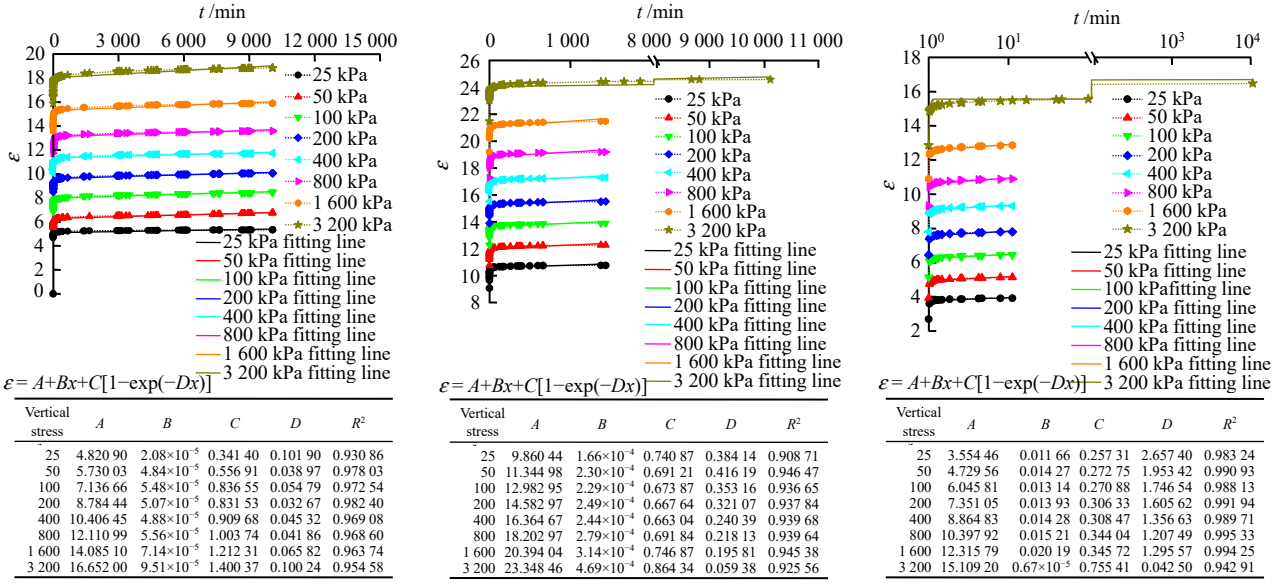

Vertical stress	A	B	C	D	R^2
25	4.820 90	2.08×10^{-5}	0.341 40	0.101 90	0.930 86
50	5.730 03	4.84×10^{-5}	0.556 91	0.038 97	0.978 03
100	7.136 66	5.48×10^{-5}	0.836 55	0.054 79	0.972 54
200	8.784 44	5.07×10^{-5}	0.831 53	0.032 67	0.982 40
400	10.406 45	4.88×10^{-5}	0.909 68	0.045 32	0.969 08
800	12.110 99	5.56×10^{-5}	1.003 74	0.041 86	0.968 60
1 600	14.085 10	7.14×10^{-5}	1.212 31	0.065 82	0.963 74
3 200	16.652 00	9.51×10^{-5}	1.400 37	0.100 24	0.954 58

(a) T1 test

Vertical stress	A	B	C	D	R^2
25	9.860 44	1.66×10^{-4}	0.740 87	0.384 14	0.908 71
50	11.344 98	2.30×10^{-4}	0.691 21	0.416 19	0.946 47
100	12.982 95	2.29×10^{-4}	0.673 87	0.353 16	0.936 65
200	14.582 97	2.49×10^{-4}	0.667 64	0.321 07	0.937 84
400	16.364 67	2.44×10^{-4}	0.663 04	0.240 39	0.939 68
800	18.202 97	2.79×10^{-4}	0.691 84	0.218 13	0.939 64
1 600	20.394 04	3.14×10^{-4}	0.746 87	0.195 81	0.945 38
3 200	23.348 46	4.69×10^{-4}	0.864 34	0.059 38	0.925 56

(b) T2 test

Vertical stress	A	B	C	D	R^2
25	3.554 46	0.011 66	0.257 31	2.657 40	0.983 24
50	4.729 56	0.014 27	0.272 75	1.953 42	0.990 93
100	6.045 81	0.013 14	0.270 88	1.746 54	0.988 13
200	7.351 05	0.013 93	0.306 33	1.605 62	0.991 94
400	8.864 83	0.014 28	0.308 47	1.356 63	0.989 71
800	10.397 92	0.015 21	0.344 04	1.207 49	0.995 33
1 600	12.315 79	0.020 19	0.345 72	1.295 57	0.994 25
3 200	15.109 20	0.67×10^{-5}	0.755 41	0.042 50	0.942 91

(c) T3 test

Fig. 5 ε–t curves in loading stages in T1, T2 and T3 tests

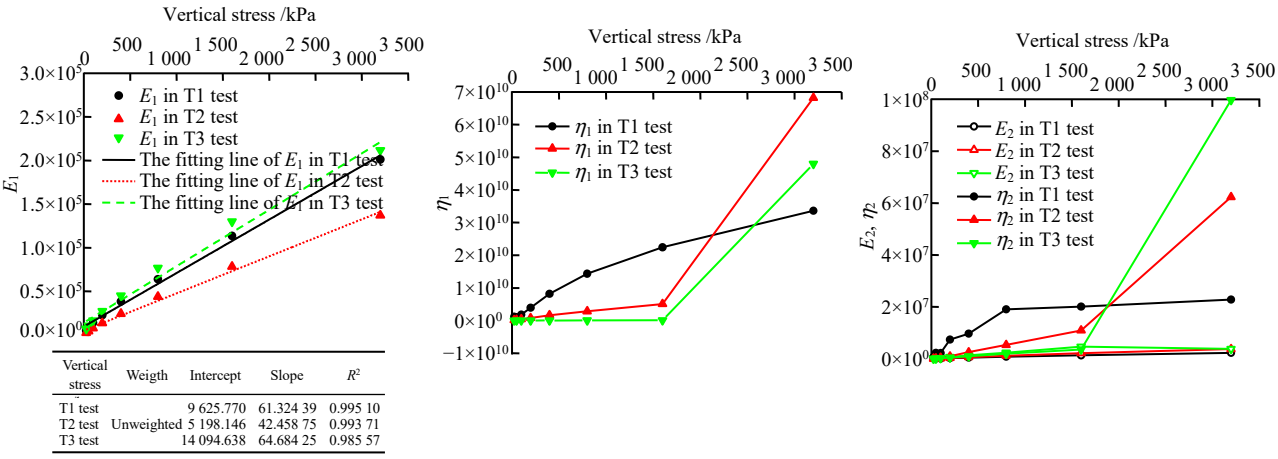

Vertical stress	Weigth	Intercept	Slope	R^2
T1 test		9 625.770	61.324 39	0.995 10
T2 test	Unweighted	5 198.146	42.458 75	0.993 71
T3 test		14 094.638	64.684 25	0.985 57

(a) E_1 (b) η_1 (c) E_2, η_2

Fig. 6 Burgers model parameters in loading stages in T1, T2 and T3 tests

It should be pointed out that the t_1 value of ε–t curve in the unloading stage was different from that in the loading stage, and the loading time t just took into account the load in current stage, t was 1 440 min when σ ranged from 200 to 1 600 kPa, and it ranged from 0 to 1 440 min. and t was 11 520 min when σ was 3 200 kPa, and it ranged from 0 to 11 520 min. The t_1 in the unloading stage was the unloading time in the previous load stages.

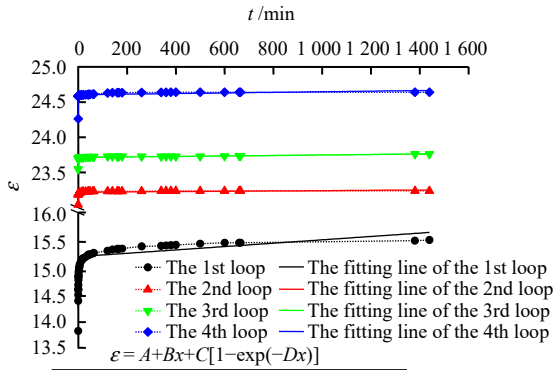

Vertical stress	A	B	C	D	R^2
The 1st loop	14.583	2.492×10^{-4}	0.668	0.321	0.937 84
The 2nd loop	21.188	6.584×10^{-6}	0.041	0.129	0.963 81
The 3rd loop	23.686	2.717×10^{-5}	0.032	0.430	0.971 51
The 4th loop	24.588	5.370×10^{-7}	0.051	0.014	0.971 37

(a) Load to 200 kPa

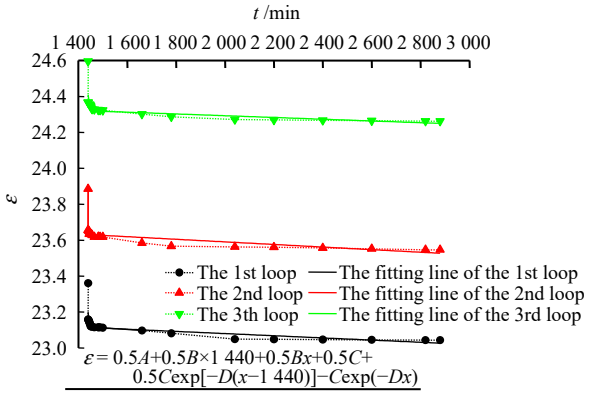

Vertical stress	A	B	C	D	R^2
The 1st loop	23.212	-5.443×10^{-5}	0.053	0.093	0.957 19
The 2nd loop	23.588	-2.554×10^{-5}	0.068	0.015	0.975 14
The 3rd loop	24.320	-2.934×10^{-5}	0.064	0.023	0.976 39

(b) Unload to100 kPa

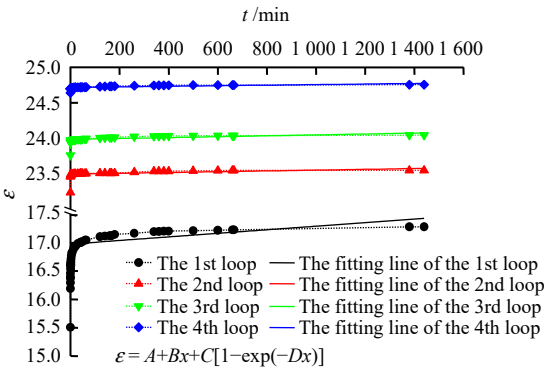

Vertical stress	A	B	C	D	R^2
The 1st loop	16.365	2.445×10^{-4}	0.663	0.240	0.939 68
The 2nd loop	23.465	4.319×10^{-5}	0.039	0.299	0.869 26
The 3rd loop	23.962	1.772×10^{-5}	0.059	0.013	0.927 50
The 4th loop	24.704	9.125×10^{-6}	0.038	0.009	0.948 30

(c) Load to 400 kPa

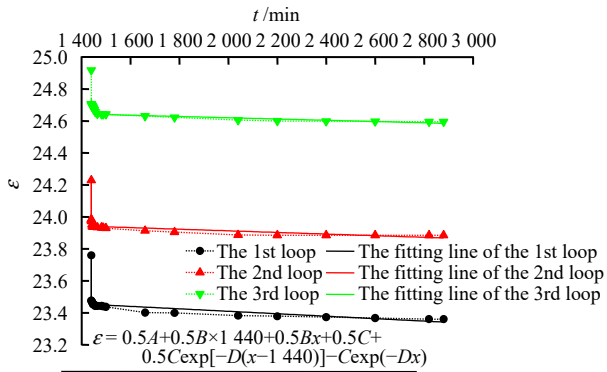

Vertical stress	A	B	C	D	R^2
The 1st loop	23.447	-3.480×10^{-5}	0.061	0.016	0.977 37
The 2nd loop	23.999	-4.151×10^{-5}	0.052	0.343	0.940 29
The 3rd loop	24.656	-3.216×10^{-5}	0.072	0.057	0.987 36

(d) Unload to200 kPa

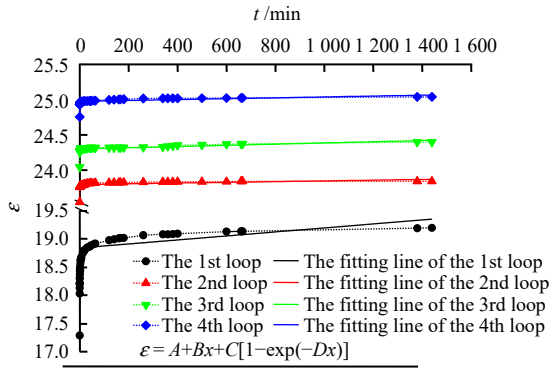

Vertical stress	A	B	C	D	R^2
The 1st loop	18.203	2.791×10^{-4}	0.692	0.218	0.939 64
The 2nd loop	23.766	1.379×10^{-5}	0.060	0.040	0.977 19
The 3rd loop	24.259	6.830×10^{-5}	0.055	0.304	0.964 14
The 4th loop	24.934	4.681×10^{-5}	0.053	0.250	0.908 34

(e) Load to 800 kPa

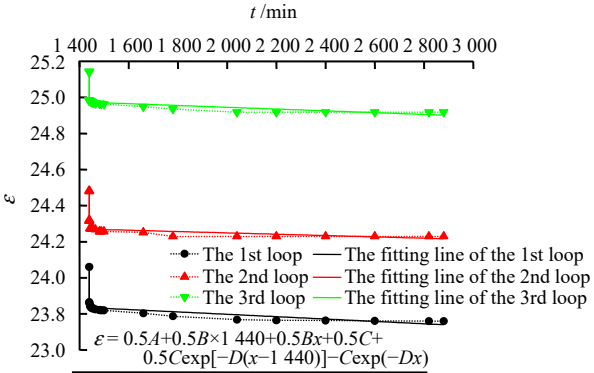

Vertical stress	A	B	C	D	R^2
The 1st loop	23.903	-4.739×10^{-5}	0.049	0.095	0.958 43
The 2nd loop	24.287	-2.916×10^{-5}	0.059	0.335	0.922 97
The 3rd loop	24.873	-3.312×10^{-6}	0.059	0.005	0.982 66

(f) Unload to400 kPa

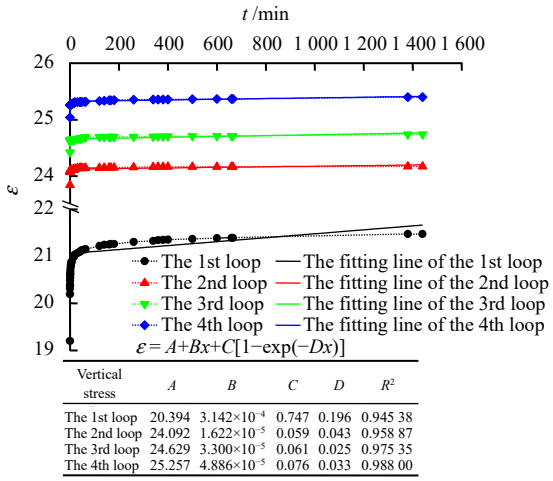

Vertical stress	A	B	C	D	R^2
The 1st loop	20.394	3.142×10^{-4}	0.747	0.196	0.945 38
The 2nd loop	24.092	1.622×10^{-5}	0.059	0.043	0.958 87
The 3rd loop	24.629	3.300×10^{-5}	0.061	0.025	0.975 35
The 4th loop	25.257	4.886×10^{-5}	0.076	0.033	0.988 00

(g) Load to 1 600 kPa

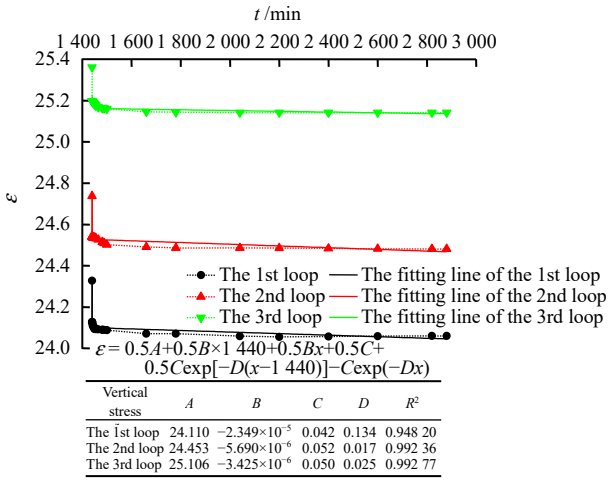

Vertical stress	A	B	C	D	R^2
The 1st loop	24.110	-2.349×10^{-5}	0.042	0.134	0.948 20
The 2nd loop	24.453	-5.690×10^{-6}	0.052	0.017	0.992 36
The 3rd loop	25.106	-3.425×10^{-6}	0.050	0.025	0.992 77

(h) Unload to 800 kPa

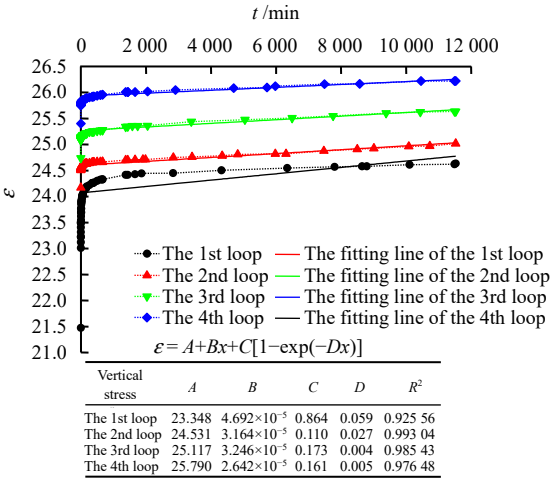

Vertical stress	A	B	C	D	R^2
The 1st loop	23.348	4.692×10^{-5}	0.864	0.059	0.925 56
The 2nd loop	24.531	3.164×10^{-5}	0.110	0.027	0.993 04
The 3rd loop	25.117	3.246×10^{-5}	0.173	0.004	0.985 43
The 4th loop	25.790	2.642×10^{-5}	0.161	0.005	0.976 48

(i) Load to 3 200 kPa

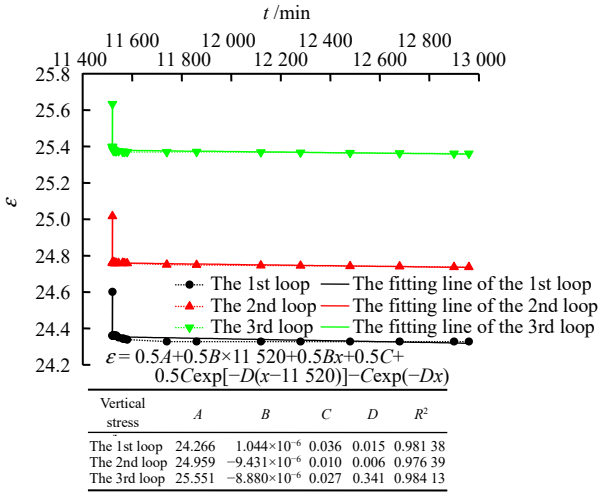

Vertical stress	A	B	C	D	R^2
The 1st loop	24.266	1.044×10^{-6}	0.036	0.015	0.981 38
The 2nd loop	24.959	-9.431×10^{-6}	0.010	0.006	0.976 39
The 3rd loop	25.551	-8.880×10^{-6}	0.027	0.341	0.984 13

(j) Unload to 1 600 kPa

Fig. 7 ε–t curves under different loading-unloading loops in T2 test

When load decreased to 100 and 800 kPa, the previous load lasts 1 440 min, and t_1 ranged from 1 440 to 2 880 min. When the load decreased to 1 600 kPa, the previous load lasted 11 520 min, and t_1 ranged from 11 520 to 12 960 min.

According to A, B, C, and D in Fig. 7, the Burgers model parameters E_1, E_2, η_1, η_2 of T2 test in the loading-unloading stage were obtained, where all the values of the viscosity coefficient η_1 in the unloading stage were negative, indicating that the deformation of Newton dashpot in Maxwell body is treated as rebound deformation in the unloading stage in the classical Burgers model. It goes against that the deformation of Newton dashpot cannot be recovered completely after unloading[24], so the classical Burgers body has its own defects in the unloading stage. Although the fitting accuracy is high, parameter η_1 has lost its physical meaning and cannot reflect the long-term deformation characteristics of the coral mud accurately, then further improvement is needed.

4.4 Improved Burgers model and its parameters

Since the defects of Burgers model in the unloading stage affect the results, the classical Burgers model was further improved in this paper.

The improved Burgers model was divided into two stages: loading stage and unloading stage. The model parameters in loading stage could still use the results in Figs. 6 and 7. Considering that the deformation of Newton dashpot was unrecoverable after unloading in Maxwell body and the loading-unloading ratio of T2 test was 1, the η_1 value of the loading stage (load from σ_i to σ_{i+1}) was substituted into Eq. (7) of the corresponding unloading stage (unload from σ_{i+1} to σ_i) to improve the Burgers model, and then the ε–t curve of Fig.7 in the unloading stage was refitted, all the values of R^2 were greater than 0.9. The model parameters E_1, E_2, η_1, η_2 of the T2 test were obtained by the improved Burgers model, as shown

in Fig. 8.

4.5 Physical meaning of improved Burgers model parameters

Analyzing the model parameters in the loading stage showed that the elastic modulus E_1 was related to the instantaneous deformation of the soil at the loading moment, and the other three parameters were related to the delayed deformation. Based on Eq. (2), the relationship between strain rate $\varepsilon_{\mathrm{p}}'(t)$ and time t in loading stage could be obtained by derivative of t:

$$\varepsilon_{\mathrm{p}}'(t)=\frac{\sigma}{\eta_1}+\frac{\sigma}{E_2}\left[\frac{E_2}{\eta_2}\mathrm{e}^{\left(-\frac{E_2}{\eta_2}t\right)}\right] \tag{9}$$

When $t\to\infty$,

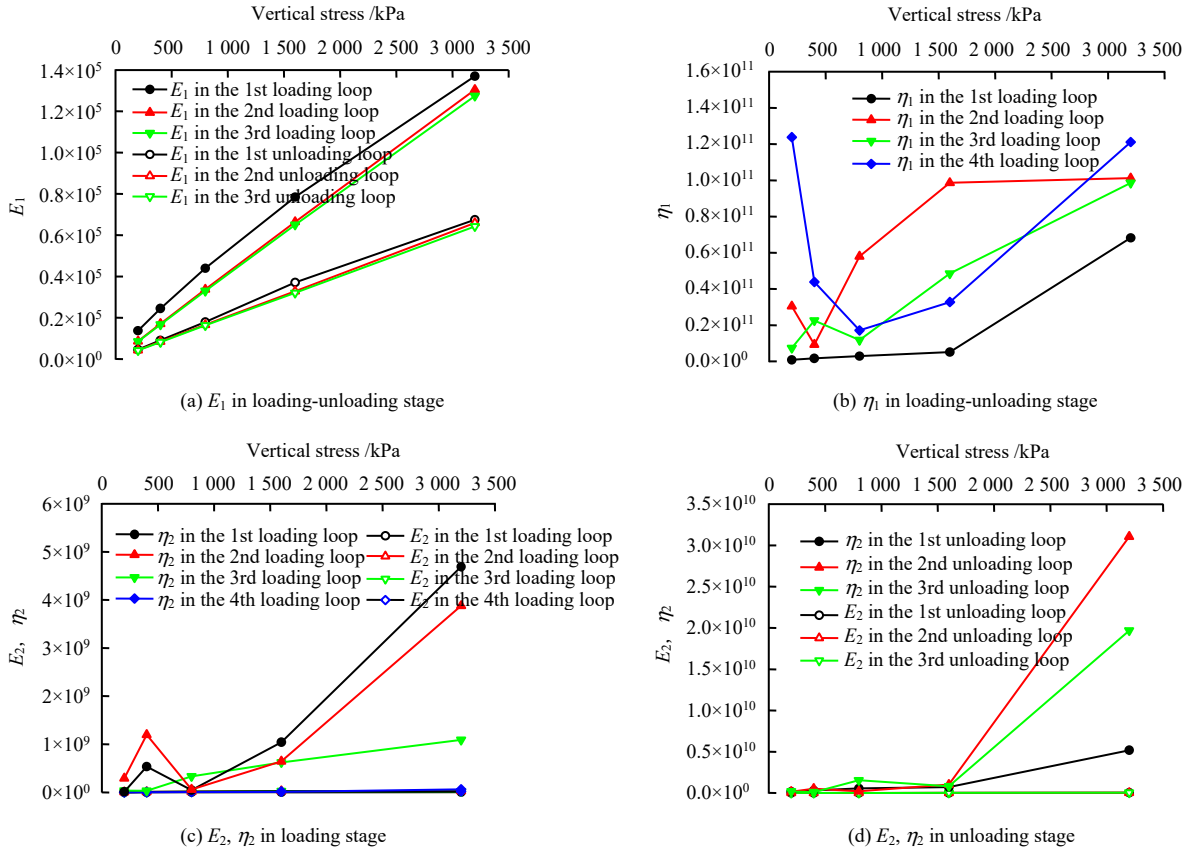

(a) E_1 in loading-unloading stage

(b) η_1 in loading-unloading stage

(c) E_2, η_2 in loading stage

(d) E_2, η_2 in unloading stage

Fig. 8 Improved Burgers model parameters in T2 test

$$\varepsilon_{\mathrm{p}}'(t)\Big|_{t\to\infty}=\frac{\sigma}{\eta_1} \tag{10}$$

Taking the further derivative of t according to Eq. (9), we could obtain:

$$\varepsilon_{\mathrm{p}}''(t)=-\frac{\sigma}{E_2}\left(\frac{E_2}{\eta_2}\right)^2\mathrm{e}^{\left(-\frac{E_2}{\eta_2}t\right)} \tag{11}$$

It can be seen that the long-term deformation characteristics of soil in the loading stage could be characterized by the model parameters E_1, E_2, η_1, η_2. The instantaneous deformation of soil was related to the elastic modulus E_1 in the instantaneous deformation stage. In the delayed attenuation deformation stage, the strain rate $\varepsilon_{\mathrm{p}}''(t)$ was always less than 0 according to Eq. (11), and decreased with time. The soil demonstrated the delayed attenuation characteristics, which is related to the elastic modulus E_2 and the viscosity coefficient η_2. In the delayed stable deformation stage, the soil demonstrated delayed stable deformation according to Eq. (10). When t tended to infinity, the strain rate tended to a constant value σ/η_1, which is consistent with the conclusion drawn from Vienna 1D oedometer test[25] that long-term deformation persists without disappearing. The strain rate decreased with the increase of viscosity coefficient η_1 under the same vertical stress.

Analysis of the model parameters in the unloading stage indicated that the elastic modulus E_1 was related to the instantaneous deformation of the soil at the unloading moment, and the other three parameters were related to the delayed deformation. Taking derivative of Burgers unloading constitutive Eq. (7) with respect to t yield:

$$\varepsilon_{\mathrm{r}}'(t)=\frac{1}{2}\frac{\sigma}{\eta_1}-\frac{1}{2}\frac{\sigma}{E_2}\frac{E_2}{\eta_2}\mathrm{e}^{-\frac{E_2}{\eta_2}(t-t_1)}+\frac{\sigma}{E_2}\frac{E_2}{\eta_2}\mathrm{e}^{-\frac{E_2}{\eta_2}t} \tag{12}$$

When $t\to\infty$,

$$\varepsilon_{\mathrm{r}}'(t)=\frac{1}{2}\frac{\sigma}{\eta_1} \tag{13}$$

Taking the further derivative of Eq. (12) with respect to t gives:

$$\varepsilon_{\mathrm{r}}''(t)=\frac{1}{2}\frac{\sigma}{E_2}\left(\frac{E_2}{\eta_2}\right)^2 \mathrm{e}^{-\frac{E_2}{\eta_2}(t-t_1)}-\frac{\sigma}{E_2}\left(\frac{E_2}{\eta_2}\right)^2 \mathrm{e}^{-\frac{E_2}{\eta_2}t} \tag{14}$$

According to the unloading curve in Fig. 7, $\varepsilon_{\mathrm{r}}''(t)>0$ as t ranged from 1 440 to 1 570 min, the unloading curve was convex downwards.

The model parameters E_1, E_2, η_1, η_2 in the unloading stage were similar with that in the loading stage. It can be seen from Eq. (13) that the delayed stable strain rate of soil tends to a constant value $\sigma/2\eta_1$ with time.

4.5.1 Effect of graded loading time on 1D long-term deformation of coral mud

Based on the physical meaning of the model parameters in the loading stage of T1, T2 and T3 tests, the effect of graded loading time on the 1D long-term deformation properties of coral mud is analyzed.

Figure 6(a) illustrates that the elastic modulus E_1 of the three tests is proportional to the vertical stress σ. The instantaneous strain increment of soil was analyzed, as shown in Fig. 9. When the graded loading time was increased by 140 times, the growth rate of the instantaneous strain increment of T2 test was about 0.34 to 0.84 times that of T3 test; when the graded loading time was increased by 1 000 times, the growth rate of T1 test was about 0.15 to 0.67 times that of T3 test. Therefore, increasing the graded loading time could effectively reduce the instantaneous strain increment and its growth rate.

When analyzing the deformation characteristics of soil in the delayed attenuation stage, one could see from Eq. (9) that the change of soil strain rate was mainly controlled by the elastic modulus E_2 and the viscosity coefficient η_2. The strain rate tended to a constant value σ/η_1 at a certain time after loading, the delayed attenuation stage was over at this moment, and the soil was in the delayed stable deformation stage. The following equation was proposed to analyze the relationship between the duration of delayed attenuation deformation and the vertical stress, elastic modulus E_2 and viscosity coefficient η_2:

$$t_{\mathrm{a}}=\frac{\sigma}{E_2}\left(a\frac{\eta_2}{\sigma}+bt_0\right) \tag{15}$$

where t_{a} is the duration of delayed attenuation deformation (min); a and b are parameters; and t_0 is the reference time, $t_0=0.1$ min.

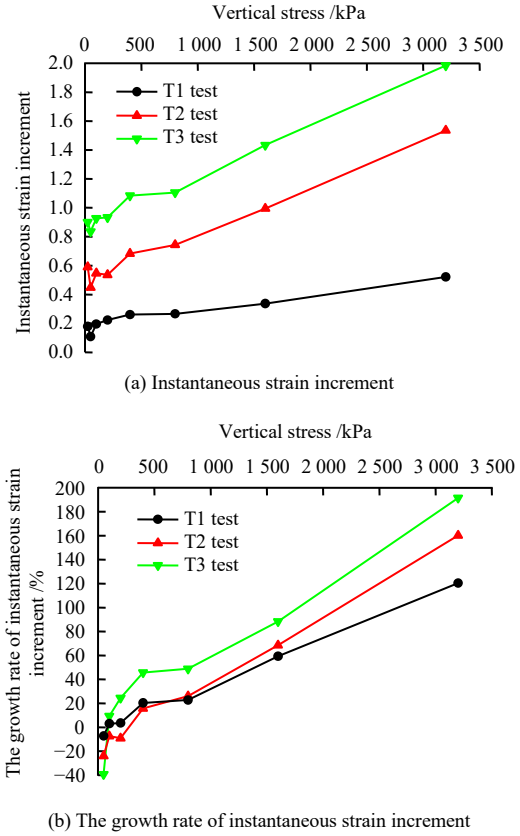

Fig. 9 Instantaneous strain increment and its growth rate in T1, T2 and T3 tests

The fitting results of Eq. (15) are shown in Table 3, and all the values of R^2 are greater than 0.95. Parameter a decreases with the increase of graded loading time while parameter b does the opposite.

Table 3 Fitting results of t_{a} with σ, E_2 and η_2 in the tests

Order number	a	b	Correlation coefficient R^2
T1	19.804 39	229 033.167 6	0.998 20
T2	21.330 75	6 881.254 5	0.996 72
T3	25.923 84	−254 079.901 9	0.999 82

Figure 10 illustrates that the duration of delayed attenuation deformation increases with the increase of the graded loading time when the vertical stress is small, while it decreases when the vertical stress is maximum, indicating that the soil particles are arranged tightly under a longer loading time in the early loading stage, and the duration of delayed attenuation deformation increases, whereas the soil particles are difficult to move under the final load, the duration of delayed attenuation deformation decreases, and the soil is in the delayed stable deformation stage quickly.

Figures 6(b) and 11 demonstrate that the viscosity coefficient η_1 of T1 test is the maximal when the vertical stress is small, followed by T2, and T3 is the minimal.

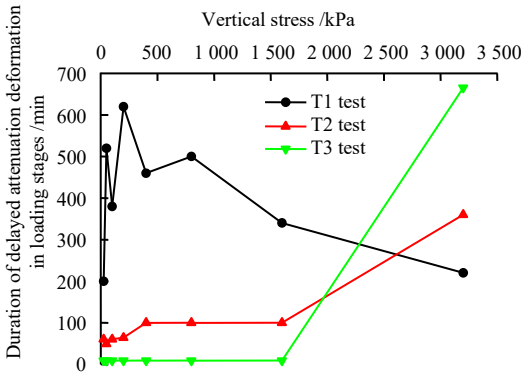

Fig. 10 Duration of delayed attenuation deformation in loading stages in T1, T2 and T3 tests

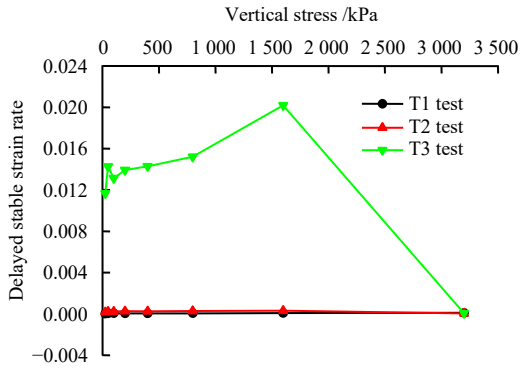

Fig. 11 Delayed stable strain rate in loading stages in T1, T2 and T3 tests

The delayed stable strain rates of T1 and T2 test are far less than that of T3 test at this moment. When the vertical stress is large, the delayed stable strain rates of the three are similar and tend to zero. Therefore, increasing the graded loading time can effectively reduce the delayed stable strain rate of soil.

Comparing the total strain increment under the final load of 3 200 kPa in the three tests in Fig. 3, it was found that the values in T1, T2, and T3 tests were 2.964%, 2.995%, and 3.612%, respectively. Increasing the graded loading time could reduce the long-term deformation of soil to a certain extent under graded loading according to the above soil deformation.

4.5.2 Effect of loading-unloading loops on 1D long-term deformation of coral mud

Based on the physical meaning of the model parameters in loading-unloading stage of T2 test, the effect of the loading-unloading loops on the 1D long-term deformation of coral mud was analyzed.

Figure 12 illustrates that the instantaneous strain increment of soil in the unloading stage is smaller than that in the loading stage under the same loading-unloading loops and vertical stress. According to Fig. 3(c), both of the instantaneous strain increments in the loading-unloading stages are similar and decrease with the increase of the loading-unloading loops.

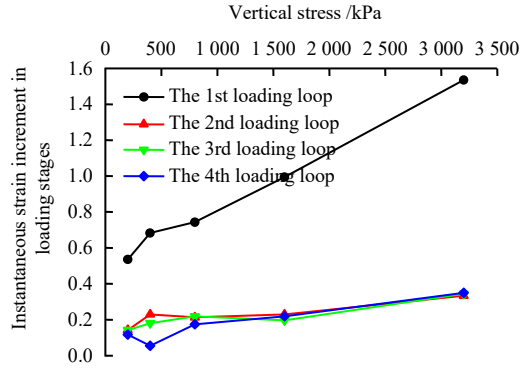

(a) Instantaneous strain increment in loading stages

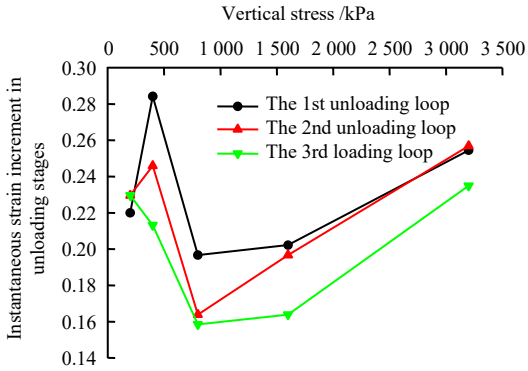

(b) Instantaneous strain increment in unloading stages

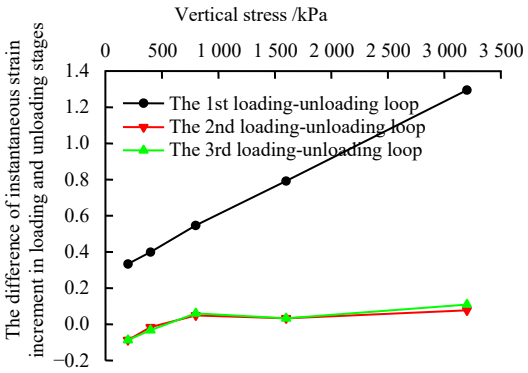

(c) The difference of instantaneous strain increment in loading and unloading stages

Fig. 12 Instantaneous strain increment in loading and unloading stages in T2 test

Equation (15) was used to fit the relationship between the duration of delayed attenuation deformation and vertical stress, elastic modulus E_2, and viscosity coefficient η_2 under different loops, as shown in Table 4, it shows a high fitting accuracy. Parameter a first decreases and then increases with the increase of the loading-unloading loops, while parameter b first increases and then decreases.

Figure 13 shows that the duration of delayed attenuation deformation in the loading-unloading stages decreases

with the increase of the loading-unloading loops, indicating that the arrangement of soil particles tends to the stable state under repeated loading-unloading loops, and the soil enters the delayed stable deformation stage faster.

Table 4 Fitting results of t_a with σ, E_2 and η_2 in T2 test

Loading-unloading loops	*a*	*b*	Correlation coefficient R^2
The 1st loading loop	21.364 86	1 757.553 9	0.996 31
The 2nd loading loop	7.438 35	27 410 900.000 0	0.855 55
The 3rd loading loop	9.419 67	8 055 815.019 5	0.928 28
The 4th loading loop	17.579 19	−5 760 480.734 8	0.994 98
The 1st unloading loop	14.032 92	−3 451 387.183 3	0.995 32
The 2nd unloading loop	12.341 19	119 553 000.000 0	0.886 22
The 3rd unloading loop	14.199 28	17 474 600.000 0	0.999 17

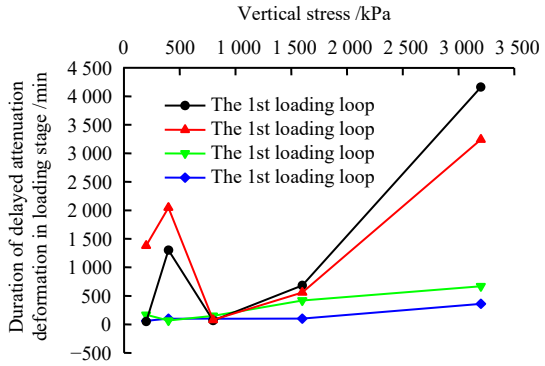

(a) Duration of delayed attenuation deformation in loading stage

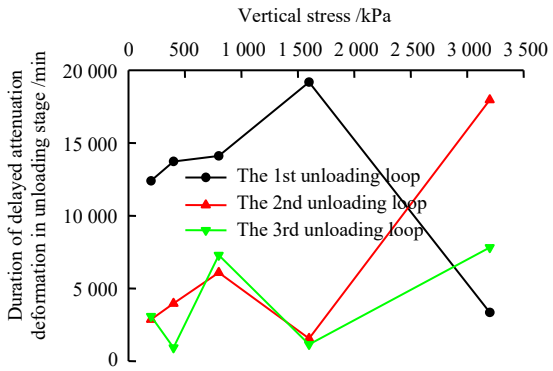

(b) Duration of delayed attenuation deformation in unloading stage

Fig. 13 Duration of delayed attenuation deformation in T2 test

Figures 8 (b) and 14 show that the viscosity coefficient η_1 of the first loading-unloading loop is the smallest under the same vertical stress, and the delayed stable strain rate is the largest. The delayed stable strain rate decreases rapidly and is close to zero with the increase of loading-unloading loops.

According to Figs. 3(b) and 3(c), the total strain increments at 3 200 kPa for each loading-unloading loop of T2 test were compared. It was found that the strain increment values of the first, second, third loops were 2.995%, 0.896%, and 0.847% respectively. According to the above deformation characteristics of soil in three stages under loading and unloading condition, increasing the loading-unloading loops can reduce the long-term deformation of soil to a certain extent.

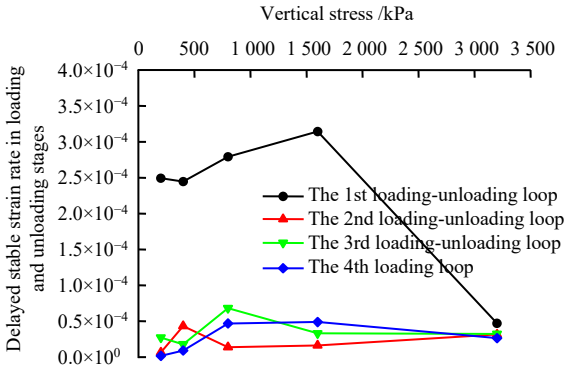

Fig. 14 Delayed stable strain rate in loading and unloading stages in T2 test

5 Conclusions

(1) The characteristics of the South China Sea coral mud, such as irregular particle morphology and high void ratio, make it quite different from the general weak clay. This paper investigates the long-term deformation properties of coral mud in the loading-unloading stage through 1D oedometer tests with different loading and unloading schemes. According to the variation of the ε–t test curve, the improved Burgers model is used to fit the curve, and the high fitting accuracy is obtained, indicating that the model can well reflect the instantaneous deformation, delayed attenuation deformation and delayed stable deformation of coral mud.

(2) The physical meaning of coral mud in each deformation stage is further explored by the improved Burgers model parameters. E_1 reflects the instantaneous deformation and can represent the instantaneous strain increment. E_2 and η_2 reflect the delayed attenuation deformation and can represent the duration of delayed attenuation deformation. η_1 reflects the delayed stable deformation and can represent the delayed stable strain rate. The larger η_1 at the same load level, the smaller the delayed stable strain rate.

(3) The instantaneous strain increment of the soil and its growth rate decrease with the increase of the graded loading time, the duration of delayed attenuation deformation under the final load decreases, the delay stable strain rate and the total strain increment under the final load decrease, so increasing the graded loading time can reduce the long-term deformation of the coral mud.

(4) The instantaneous strain increment in the unloading

stage is smaller than that in the loading stage under the same loading-unloading loops and vertical stress. The instantaneous strain increments at loading and unloading moments are similar and decreases with the increase of loading-unloading loops. The duration of delayed attenuation deformation in loading-unloading stage is reduced; and the delayed stable strain rate and the total strain increment under the final load decrease, so increasing the loading-unloading loops can reduce the long-term deformation of coral mud.

(5) The long-term nonlinear deformation of the South China Sea coral mud can be effectively weakened by increasing graded loading time and the loading-unloading loops. Therefore, extending the graded loading time and increasing the loading-unloading loops may enhance the long-term stability of the reclaimed island and reef foundation in the preloading scheme of actual project.

References

[1] WANG Ren, WU Wen-juan. Exploration and research on engineering geological properties of coral reefs——Engaged in coral reef research for 30 years[J]. Journal of Engineering Geology, 2019, 27(1): 202−207.

[2] YUAN Zheng, YU Ke-fu, WANG Ying-hui, et al. Research progress in the engineering geological characteristics of coral reefs[J]. Tropical Geography, 2016, 36(1): 87−93.

[3] WANG Xin-zhi, WANG Xing, LIU Hai-feng, et al. Field test study of engineering behaviors of coral reef foundation[J]. Rock and Soil Mechanics, 2017, 38(7): 2065−2079.

[4] YIN Jian-hua, CLARK J I. One-dimensional time dependent stress-strain behaviour of soils, elastic visco-plastic modelling, and consolidation analysis[J]. Rock and Soil Mechanics, 1994, 15(3): 65−80.

[5] MESRI G, GODLEWSKI P M. Time-compressibility and stress-compressibility interrelationship[J]. Journal of the Geotechnical Engineering Division, ASCE, 1979, 105(1): 106−113.

[6] MESRI G, GODLEWSKI P M. Time and stress compressibility interrelationship[J]. Journal of Geotechnical Engineering, 1979, 103(5): 417−430.

[7] MESRI G, FEBRESCORDERO E, SHIELDS D R, et al. Shear stress-strain-time behaviour of clays[J]. Geotechnique, 1981, 31(4): 537−552.

[8] LADD C, FOOTT R, ISHIHARA K, et al. Stress-deformation and strength characteristics: state of the art report[C]//Proceedings of 9th International Conference on Soil Mechanics and Foundation Engineering. Tokyo: [s. n.]: 1977.

[9] BJERRUM L. Engineering geology of Norwegian normally consolidated marine clays as related to the settlements of buildings[J]. Geotechnique, 1967, 17(2): 83−118.

[10] GRAHAM J, CROOKS J H, BELL A L. Time effects on the stress-strain behavior of natural soft clays[J]. Geotechnique, 1983, 33(3): 327−340.

[11] YIN J H. Calculation of settlements of foundation soils considering creep[C]//Proceedings of the Nakase Memorial Symposium. Boca Raton: CRC Press, 2003: 205−211.

[12] YIN J H, GRAHAM J. Equivalent times and one-dimensional elastic viscoplastic modelling of time-dependent stress-strain behaviour of clays[J]. Canadian Geotechnical Journal, 1994, 31(1): 42−52.

[13] YIN J H. Non-linear creep of soils in oedometer tests[J]. Geotechnique, 1999, 49(5): 699−707.

[14] YIN J H, TONG F. Constitutive modeling of time-dependent stress-strain behaviour of saturated soils exhibiting both creep and swelling[J]. Canadian Geotechnical Journal, 2011, 48(12): 1870−1885.

[15] FENG W Q, LALIT B, YIN Z Y, et al. Long-term non-linear creep and swelling behavior of Hong Kong marine deposits in oedometer condition[J]. Computers and Geotechnics, 2017, 84: 1−15.

[16] HU Hui-hua, HE Jian-qing, NIE Shi-cheng. One-dimensional consolidation creep model for sandy grain muddy soil of Dongting Lake[J]. Rock and Soil Mechanics, 2022, 43(5): 1269−1276.

[17] WANG Yuan-zhan, WANG Ting-ting, WANG Jun. A nonlinear rheological model of soft clay and its application to Tianjin littoral area[J]. Rock and Soil Mechanics, 2009, 30(9): 2679−2685.

[18] TAYLOR D W, MERCHANT W. A theory of clay consolidation accounting for secondary compression[J]. Journal of Mathematics and Physics, 1940, 19(3): 167−185.

[19] YIN De-shun, REN Jun-juan, HE Cheng-liang, et al. A new rheological model element for geomaterials[J]. Chinese Journal of Rock Mechanics and Engineering, 2007, 26(9): 1899−1903.

[20] LIU Zhong-yu, YANG Qiang. One-dimensional rheological consolidation analysis of saturated clay using fractional order Kelvin's model[J]. Rock and Soil Mechanics, 2017, 38(12): 3680−3697.

[21] LIU Qing-bing, WANG Shun, XIA Dong-sheng, et al. Experimental study of residual-state creep behavior of intact sliding-zone soil[J]. Rock and Soil Mechanics, 2017, 38(5): 1305−1313.

[22] CHEN Xiao-ping, BAI Shi-wei. Research on creep-consolidation characteristics and calculating model of soft soil[J]. Chinese Journal of Rock Mechanics and Engineering, 2003, 22(5): 728−734.

[23] SHEN Yang, FENG Zhao-yan, LIU Han-long, et al. Experimental study on effects of initial concentration on settling velocity characteristics of turbid surface of South China Sea coral mud[J]. Chinese Journal of Geotechnical Engineering, 2018, 40(Suppl.2): 22−26.

[24] QIAN Jia-huan, YIN Zong-ze. Geotechnical theory and calculation[M]. Beijing: China Water Power Press, 1996.

[25] BRANDL H. Consolidation/creeping of soils and pre-treated sludge[J]. Poromechanics V-Proceedings of the 5th Biot Conference on Poromechanics, 2013(1): 1346−1357.